Broad bandwidth air-coupled micromachined ultrasonic transducers for gas sensing

P. Shanmugam, L. Iglesias, J.F. Michaud, Daniel Alquier, L. Colin, I. Dufour, D. Certon

BROAD BANDWIDTH AIR-COUPLED MICROMACHINED ULTRASONIC TRANSDUCERS FOR GAS SENSING

P. Shanmugam[a,*], L. Iglesias[b], J.F. Michaud[a], D. Alquier[a], L. Colin[a], I. Dufour[b], D. Certon[a]

[a] GREMAN Laboratory UMR-CNRS 7347, University of Tours, 16 rue Pierre et Marie Curie, BP 7155, 37071 TOURS Cedex 2, France

[b] IMS Laboratory UMR-CNRS 5218, University of Bordeaux, 351 cours de la libération, 33405 TALENCE Cedex, France

*Corresponding author: priyadarshini.shanmugam@univ-tours.fr

Authors list :

Shanmugam Priyadarshini : priyadarshini.shanmugam@univ-tours.fr

Luis Iglesias : luis.iglesias-hernandez@u-bordeaux.fr

Jean François Michaud : jean-francois.michaud@univ-tours.fr

Daniel Alquier : daniel.alquier@univ-tours.fr

Laurent Colin : laurent.colin@univ-tours.fr

Isabelle Dufour : isabelle.dufour@ims-bordeaux.fr

Dominique Certon : dominique.certon@univ-tours.fr

Abstract

The present work aims to develop ultra-wide bandwidth air-coupled capacitive micromachined ultrasonic transducers (CMUTs) for binary gas mixture analysis. The detection principle is based on time-of-flight (ToF) measurements, in order to monitor gas ultrasound velocity variations. To do such measurements, CMUTs were especially designed to work out of resonance, as a microphone. The chosen membrane size is 32x32 µm² and gap height 250 nm. The resonance frequency and collapse voltage were found at 8 MHz and 58 V respectively. As mentioned, the CMUTs were exploited in quasi-static operating mode, in a very low frequency band, from 1 MHz to 1.5 MHz frequency. The transducer impulse response was characterised, and a -6 dB relative fractional frequency bandwidth (FBW) higher than 100 % was measured, enabling to use CMUT for the targeted application. Additionally, a measuring cell has been designed to hold the fabricated CMUT emitter and receiver prototypes facing each other. The volume inside the cell was kept lower than 3 mL and the surface of emitter/receiver was 1.6×8 mm^2. To validate the general principle of the proposed technique, two binary gas mixtures of CO_2/N_2 and H_2/N_2, with varying concentration, have been tested. The results are very promising with a measured limit of detection (LOD) of 0.3 % for CO_2 in N_2 and 0.15 % for H_2 in N_2.

Index terms: Capacitive micromachined ultrasonic transducers, gas sensors, air-coupled transducers, time-of-flight.

I. INTRODUCTION

Capacitive micromachined ultrasonic transducers (CMUTs) were introduced in mid 1990s by M.I. Haller and B.T. Khuri-Yakub [1], [2]. Since then, they are considered as a potential substitute to the conventional piezoelectric transducers due to their numerous advantages such as miniaturization, lead-free, relatively broad bandwidth and improved axial resolution [3]. In the beginning, CMUTs were developed for airborne applications but, rapidly, were used to address multiple applications, in particular medical ones [4]–[12]. As an example, this leads to the development of dedicated CMUT probes for cortical bone assessment [13] and dual-modality CMUT probes for imaging and therapy [14], [15]. The performances of CMUT in air applications have been underestimated for long, due to their lack of sensitivity for non-destructive testing applications [16]. Recently, new CMUT structures were designed to produce ultrasound field in the frequency range of 50 kHz – 150 kHz] [17], [18], showing encouraging performances with receiving sensitivity of 16.6 mV/Pa and fractional bandwidth up to 10 %. For the same frequency range, transducer topologies based on annular CMUTs was also proposed as an interesting approach to improve the transmit efficiency [19]–[21], where value of 70 Pa/Volt was predicted. Air-coupled CMUT transducer with a central frequency of 400 kHz was finally mentioned in the literature [22]. A bandwidth of 1 MHz was claimed in the paper but experimental results presented were not relevant enough to confirm such value. In the present work, the aim is to develop a complete air-coupled CMUT transducer to serve as a binary gas sensor that works on the time-of-flight (ToF) measurement principle. The sensing principle consists of measuring change in gas acoustic properties here, ultrasonic velocity, as already demonstrated for monitoring of human-specific lung gas exchange [23] and for the wind speed measurement [24]. In our case, the final application is the monitoring of hydrogen storage sites [25], targeting to detect gas leaks, i.e. to measure the presence of low concentration of hydrogen (typ. < 0.5 %).

The first research article on CMUT in the field of gas sensing was published in 2007 by Park *et al.* [26]. In their work, the top electrode was coated with a sensitive polymer in order to detect the molecule of interest, by increasing the vibrating plate mass and, thereby, decreasing the resonant frequency when absorbing these gas molecules. This paves the road to multiple researches that have been done and are ongoing on CMUT as a chemical/bio gas sensors [27]–[33]. However, adding sensitive coated polymer generally leads to only partial selectivity to multiple analytes. In addition, such solutions suffer from environmental effects,

which includes temperature or humidity variations but also material aging [34]. Therefore, sensors without sensitive coating are preferable in particular when long-term stability is a crucial issue and this even though their intrinsic selectivity limits applications [35]. In previous work [36], [37], we demonstrated the relevance of using an uncoated CMUT approach in order to sense binary gas mixture. In these works, the detection principle was based on monitoring the electrical anti-resonance frequency shift, caused by gas density and viscosity variations. Again, the targeted sensor was an uncoated CMUT transducer that detects ultrasonic velocity variations and, hence, gas compressibility and density variations. In this paper, a clear objective is also to demonstrate the versatility of CMUT technology for such applications and to demonstrate their ability to detect variations in density, compressibility as well as viscosity of gas medium.

It is worth to mention that the developed air-coupled CMUT transducer must meet several specifications. First, in terms of global footprint, the fabricated sensor must be as small as possible to be inserted in the dedicated measurement cell (few mL) developed previously by our group [35]–[37]. Secondly, the ultrasonic gas velocity variations have to be measured over a low travelling distance, typically few millimeters (< 10 mm), leading to very low ToF variations of ultrasonic pulses to be detected (few µs). The detection of low ultrasonic transit time variations is a quite current issue for various applications like ultrasonic flowmeters [38], the blood flow velocity [39] or tissue motion detection [40]. Whatever the application is, such ToF measurements make sense if i) the travel path corresponds to several acoustic wavelengths and ii) the transducer impulse response duration is lower than emitter - receiver transit time. This means that both working frequency and fractional frequency bandwidth (FBW) have to be high enough to meet these operating conditions. To achieve such conditions, the CMUT used in this study will have working frequency ranging between 1 MHz and 1.5 MHz with a FBW higher of 50%.

Several air-coupled transduction technologies exist in the literature; from devices based on bulk piezoelectric plate [41] to electrostatic transducers based on Mylar film vibration [42]. Recently, based on piezoelectric micromachined ultrasonic transducer (PMUT) technology, the first millimeter accurate ultra-low power ToF sensor has been launched commercially, used for proximity sensing applications with a dimension of 15 mm^2 [43], [44]. Few other PMUT applications as microphones, using ToF technique, can also be found in [45], [46]. Finally, a novel 2D flexural ultrasonic transducer array, working on ToF principle and composed of eight piezo ceramic disc elements with a total dimension of 36x36x0.25 mm^3, has been demonstrated for accurate average flow velocity [47]. One can

note that, for this work, the travelling distance was ranging from centimeter to meter scale [48], meaning the FBW of fabricated devices was not a crucial issue for the targeted applications. Typically, FBW of 20 % are enough for such working distance range. To achieve FBW values higher than 50 %, the developed air-coupled CMUTs were aimed to work like microphone, not only in reception, as shown in references [49]–[51], but also in emission mode. This design strategy is clearly novel compared with previous works where the membrane dimensions (sizes and thicknesses) were optimized to reach resonance frequencies close to the targeted working frequency [17]–[21], [52], [53]. To achieve such low resonance frequencies, the mechanical stiffness of the membrane must be adjusted, either by changing the CMUT sizes or thicknesses. However, if the diaphragm rests on a vacuum cavity, it undergoes significant mechanical deformation due to atmospheric pressure, which can cause non-functionality of CMUT (i.e. collapsed cells). There are two possible solutions to get circumventing such constraint. The first is to perforate the rear side [17], [18] of the cavity in order not to be affected by atmospheric pressure. The second is to increase the cavity height (typically up to 10 µm thick) [20], [53] to ensure that the membrane could deflect without collapsing. Therefore, the CMUT fabrication process for air applications requires specific steps that differ from those used for immersion applications. In our case, we have deliberately chosen to keep the CMUT diaphragm on a vacuum cavity (i.e. same process for immersion applications) and to exploit CMUT at working frequencies far from the resonance frequency, in a quasi-static operating mode as used for microphones. The CMUT were designed in order to keep membrane deformation amplitude as low as possible on one hand and to increase the radiated acoustic power on the other hand, using frequency of interest in the range of 1 MHz to 1.5 MHz. In former work [54], we have shown the relevance of such approach without evidencing design strategy, precise gas concentrations records and without discussion on acoustic velocity measurements. In this study, the gas concentration is monitored accurately for two different gas mixtures and compares the obtained results with theoretical predictions. Further, the limit of detection (LOD) and sensitivity of CMUT gas sensor will be presented in § IV.B.

The presented paper consists of three main sections. Section II gives an overview of the CMUTs fabrication process, CMUTs design, CMUTs packaging and the description of the measuring cell. From design considerations, one prototype was fabricated and characterised. Results are described in section III, using both electrical impedance data and electroacoustic measurements. Next, section IV presents the test of the fabricated gas sensor. To demonstrate the sensor efficiency, two gas mixtures were investigated, first carbon dioxide (CO_2) in

nitrogen (N_2) and then, hydrogen (H_2) in N_2. This work shows that the developed device enables to detect very low variations in the transit time for very low gas concentration (e.g. < 1 %).

II. DESIGN, FABRICATION, PACKAGING OF CMUT AND MEASURING CELL

A. CMUT fabrication process-flow

The silicon nitride (SiN_x) based CMUT used here was initially developed for medical imaging and therapeutic purposes [13], [55]. Although the CMUTs were manufactured using standard surface micromachining techniques [56], our group improved the process over years by distinguished choice of materials and deposition techniques [7], [9], [42], [57]. A brief process flow is illustrated in Figure 1.

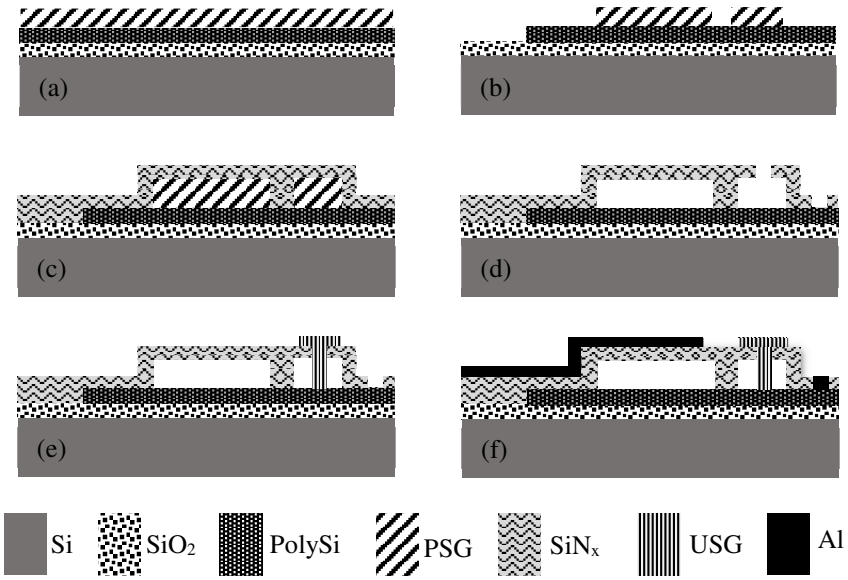

Figure 1: CMUT fabrication process flow; (a) deposition of insulation layer (SiO_2), bottom electrode (PolySi) and sacrificial layer (PSG); (b) patterning of bottom electrode and sacrificial layer; (c) deposition of membrane layer (SiN_x); (d) removal the sacrificial layer and releasing the membrane; (e) sealing the membrane; (f) deposition of top electrode (Al).

In step 1 (Figure 1.a), a 6-inch Si (100) wafer with high resistivity is used. To ensure electrical insulation of the Si substrate, a 1.2 µm thick silicon dioxide layer has been grown by thermal oxidation. Then, for bottom electrode, a 450 nm thick polycrystalline silicon (PolySi) layer has been deposited on the oxide layer using Low Pressure Chemical Vapour Deposition (LPCVD). The PolySi layer was heavily doped with POCl3 in order to ensure

high electrical conductivity. The second step consists in a crucial sacrificial layer (PhosphoSilicate Glass oxide, PSG) deposition, as its thickness defines the cavity height of the CMUT device. The step 2 (Figure 1.b) consists in a two processes: the PSG dry etching to define the membrane geometry and another etch step to define the bottom electrode (PolySi). In Step 3 (Figure 1.c), the CMUT membrane is deposited by LPCVD process, hereby a SiN_x material with thickness of 400 nm. Step 4 (Figure 1.d) is a chemical etching using hydrofluoric acid to remove the sacrificial layer and to release the membrane. Step 5 (Figure 1.e) consists in the cavity sealing and finally step 6 (Figure 1.f) correspond to aluminium top electrode deposition and patterning (450 nm). Later, the fabricated CMUTs are diced and ready for characterisation and packaging.

B. CMUT and transducer design

CMUTs were designed in such a way that they are able to work in a low frequency band, far from their own resonance frequency. In such case, they behave like a microphone and enable to obtain the broadest frequency bandwidth and lowest impulse response duration, as possible. From the previous studies, it was shown that, when CMUTs work in quasi-static regime, non-linear time-domain models enable to predict accurately the transducer response [58], [59]. The major design criterium was based on the output acoustic power radiated by the transducer. For a given 2D array of CMUTs, the output acoustic intensity (the mean spatial acoustic power) P_a is written as:

$$P_a = \frac{1}{2} R_a \left(2\pi f_0 \frac{u_0}{3}\right)^2 \quad \text{Eq. 1}$$

Where R_a, is the real part of the transducer radiation impedance, f_0 is the ultrasonic wave frequency and u_0 is the maximum peak displacement amplitude of the CMUT, taken at its center. Here, it is assumed that two-dimensional periodic boundary conditions can be applied to each CMUT, R_a, for such boundary conditions, equals to the acoustic medium impedance multiplied by the surface coverage ratio of the transducer. To consider the fact that the membrane displacement is non-uniform, a factor 1/3 was applied to obtain an approximate value of the spatial mean membrane displacement. This value was obtained through time-domain simulations, in which all details are given in reference [59].

To approximate u_0, it has been considered that, when CMUT works like a microphone, the membrane is able to sweep the whole gap height, from the static membrane position (U_i), taken at the center, up to the bottom electrode.

$$u_0 = \frac{(h_{gap} - U_i)}{2} \qquad \text{Eq. 2}$$

Where, h_{gap} is the total gap height.

By considering Eq. 1 along with the design parameters obtained from the process specifications given in Table 1, P_a was computed for square CMUT membranes, along with the spatial distribution presented in Figure 2 for dimension '*w*' ranging from 10x10 µm² to 80x80 µm².

Table 1: CMUT material parameters and thicknesses

Layer	SiN_x	Al
Thickness (nm)	400	450
E (GPa)	220	68
ν (poisson ratio)	0.22	0.35
ρ (kg/m3)	3300	2700
ε_r	7.5	

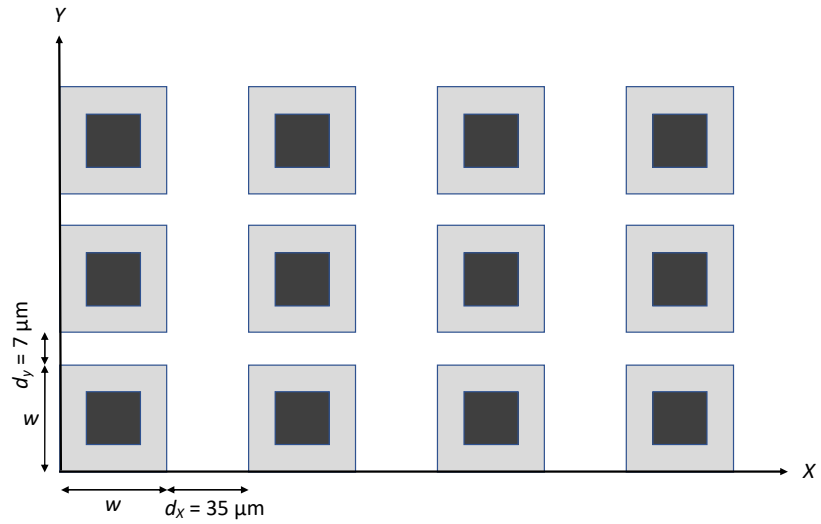

Figure 2: Sketch of CMUT distribution over the surface of the transducer, *w* is the width of each CMUT, d_x the CMUT-to-CMUT distance along *X* axis, and d_y along the *Y* axis. Black squares represent the front electrodes, the surface area of which corresponds to 50 % of the CMUT surface area

The active surface ratio was given by the parameter $w^2/(w+d_x)(w+d_y)$ as presented in Figure 2. d_x and d_y values were fixed by process specifications. More precisely, d_x is higher than d_y

because holes used to release CMUT membrane were placed along *X* axis between two CMUTs. For each membrane size, the initial deflection, caused by the atmospheric pressure, was computed with finite difference model described in [60], and the h_{gap} value was fixed to 250 nm. The computed output acoustic intensity according to the membrane size is shown in Figure 3, for two frequencies in the range of interest, i.e. 1 MHz and 1.5 MHz.

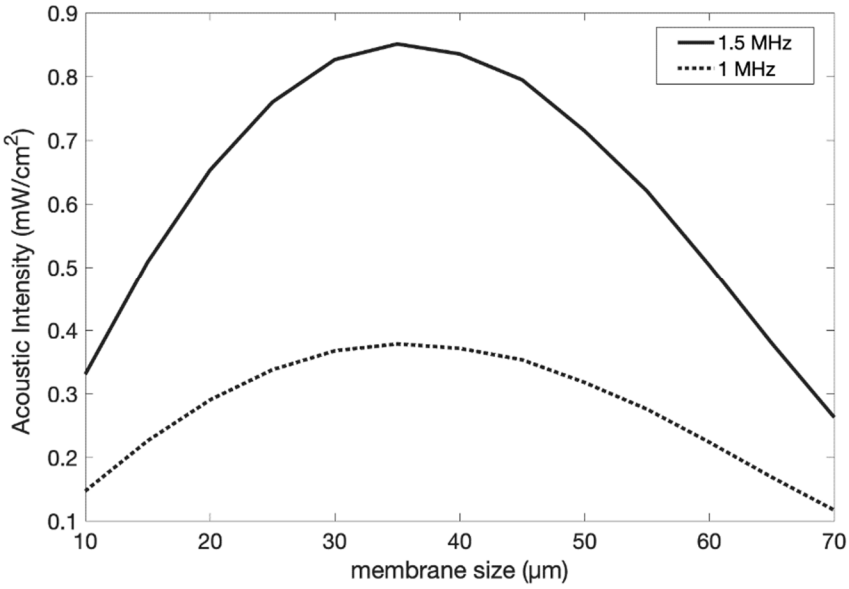

Figure 3: Computed output acoustic intensity radiated in air for square CMUTs with 2D periodic layout and membrane size ranging from 10 µm to 80 µm

Figure 3 clearly highlights the existence of an optimal size range where the acoustic intensity reaches a maximum, here it is between 30 µm and 40 µm width. This maximum comes from a trade-off between low size CMUT for which the initial deflection caused by atmospheric pressure is low and large size CMUT for which the active surface ratio is high. Hence, the final geometry retained was 32x32 μm^2. All geometrical specifications are reported in Table 2. The presented collapse voltage and resonance frequency are obtained experimentally from electrical impedance measurements and will be discussed in § III.A.

For these first experiments, since no prior knowledge on radiation surface was identified to have a suitable signal-to-noise ratio, it was targeted to fabricate an array of single element transducers for which the surface can be adjusted. Therefore, a multi-element array of eight independent acoustic emitters was fabricated. Each element was rectangle with 8 mm length and 0.8 mm width, which corresponds to 2.4 acoustic wavelength in air for 1 MHz working frequency and 3.6 wavelength at 1.5 MHz. The final number of emitters used (from 1 to 8) for

the experiments was defined from preliminary experiments presented in [54]. It was observed that pairing elements was enough for the targeted working distance, i.e. less than 10 mm.

Table 2: Specifications of the fabricated transducer

CMUT size	32x32 µm²
Gap height	250 nm
Area of top electrode	20x20 µm²
Active surface ratio	40 %
Collapse voltage (V_c)	58 V
Resonance frequency	8 MHz
Transducer length	8 mm
Element width	0.8 mm
Number of elements	8

C. CMUT packaging and measuring cell description

To package the CMUT array, a specific printed circuit board (PCB) was designed and fabricated as shown in Figure 4. The diced eight element array of size 6.4x8 mm² was glued on PCB (refer Figure 4.a) using an insulating epoxy adhesive (ALBEBOND 84-3J by Henkel) and kept in a lab oven for annealing during one hour at 150 °C. Then, wire bonding was done using K&S 4532AD manual wedge bonder with fine aluminium wedge bonding wires of 25 µm diameter. Epoxy NoSWEEP from Polysciences (wire bond encapsulant) was used to protect the bonded wires. The eight elements array was paired together to form four acoustic emitters/receivers. Then, the prototype was annealed at 100 °C and 165 °C for one hour each, to harden the encapsulation. Lastly, to complete the emitters/receivers prototype packaging, UFL connectors were soldered on the rear face of the PCB for electrical connections.

A specific measuring cell was designed as a gas sensor unit. The cell was made of acrylic monomer and fabricated using 3D printing with cubic shape. It includes two large openings, one in the front and other in the rear face (18 mm in diameter, see Figure 4.b) to conform the emission and the reception transducers. Both PCBs were positioned face-to-face to perform ToF measurements. The chamber sealing was ensured by gaskets, which were placed between the PCBs and each side of the acrylic cell to prevent gas leakage. Two small openings on the top and bottom side of the cell were kept for gas inlet and outlet respectively

(see Figure 4.c). The measuring cell was fabricated in such a way that the propagation direction of ultrasound is always perpendicular to the gas outflow.

To master precisely the concentration of binary gas mixtures, the measuring cell geometry such as height (h) (distance between emitter and receiver) and volume (V) of the inner cylinder were chosen with great care. The total volume of the inner cylinder was kept less than 3 mL in order that the filling time of the cavity be small enough to apply in real time gas concentration command. The distance between the emitter and the receiver was fixed accordingly, at a value close to 7 mm.

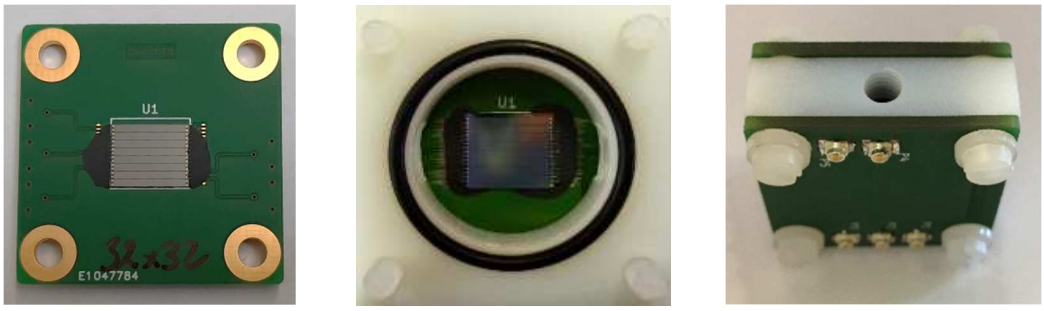

Figure 4: a) emitter/receiver prototype b) inner view of the measuring cell c) completely packed gas unit for ToF measurement

III. CMUT CHARACTERISATION RESULTS

A. Electrical impedance measurement

Electrical impedance measurement of developed CMUT devices makes it possible to extract most of the information about their electrical and mechanical behaviour. The impedance measurement protocol presented here is the same as the one shown in reference [60]. HP4294A impedance analyser, from Keysight Technology, combined with 4294A1 connected probe was used. The CMUT biasing voltage was swept automatically (with a MOTECH DC supply) from 0 to 90 V with a pitch of 2 V. For each biasing value, the electrical impedance was acquired from 1 MHz to 15 MHz, in the frequency band where mechanical resonance occurs. With the obtained data, most of the electromechanical parameters can be derived such as, capacitance at low frequency (measured at 1 MHz), resonance frequency (f_r), antiresonance frequency (f_a) and electromechanical coupling coefficient (k_t). k_t was assessed through the following approximate relationship:

$$k_t = \sqrt{\frac{f_a^2 - f_r^2}{f_a^2}} \qquad \text{Eq. 3}$$

The collapse voltage value, V_c, was determined as the voltage from which the capacitance variations suddenly drops, meaning that a part of the CMUT membrane is stuck to the bottom cavity. An experimental value of 58 V was found for the 32x32 µm² cells. Note that more than ten prototypes were realized and the collapse voltage was the same for each.

Electrical impedance measurements for three biasing voltages are plotted in Figure 5, with a focus around the resonance frequency. CMUT works as expected, i.e. the electrical anti-resonance frequency decreases on increasing the biasing voltage. The mechanical resonance frequency can be extracted at very low biasing voltage value; one can guess a value close to 8 MHz. Figure 6 demonstrates the electromechanical coupling coefficient, which increases by increasing the bias voltage and reaches a maximum of 60 %, just before collapse event.

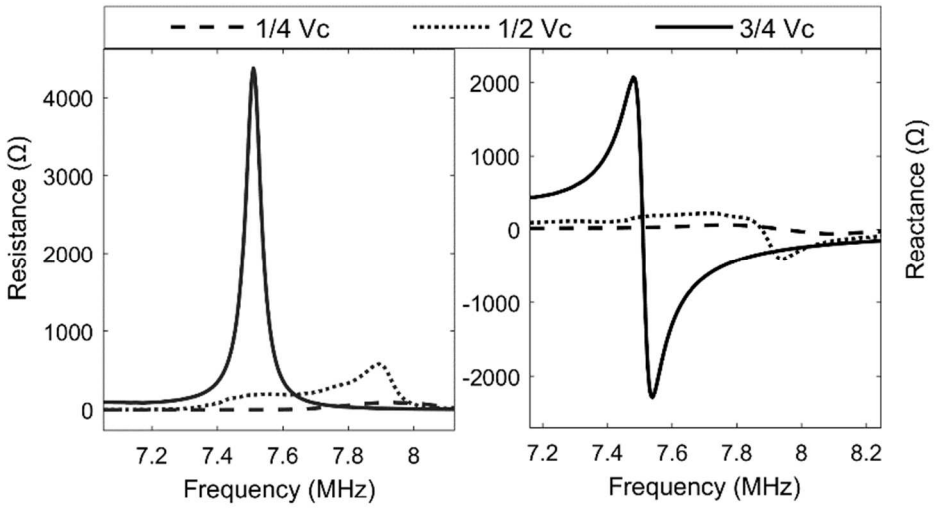

Figure 5 : Electrical impedance measurement results of single element CMUT in air

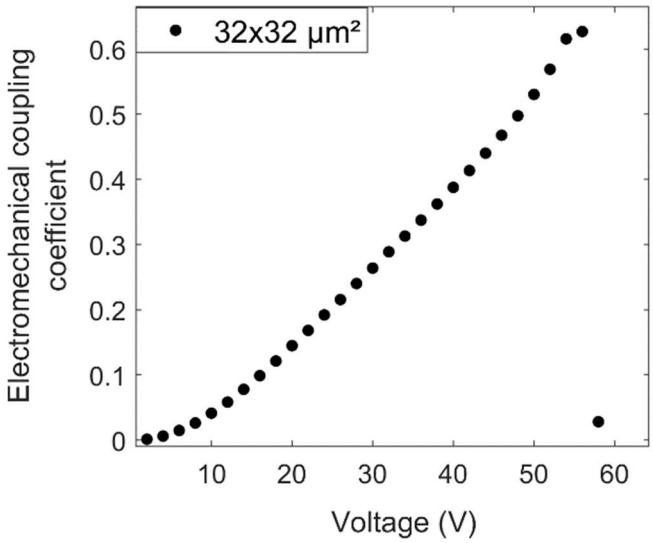

Figure 6 : Experimental electromechanical coupling coefficient of CMUT according to the biasing voltage

B. Electroacoustic characterization in air

The ultrasound ToF measurement was initially performed in air before testing in gas medium, to check several parameters such as maximum distance between emitter and receiver, emission frequency (f_e), as well as the quality of the received signals in terms of signal-to-noise ratio. For the operating excitation conditions, biasing voltage value was fixed at 70 % of V_c (i.e. 40 V) and the excitation voltage was one period of sinus-pulse with an amplitude of 30 % of its V_c (amplitude of 15 V). Five working frequencies were tested 500 kHz, 1 MHz, 1.5 MHz, 2 MHz and 3 MHz. Emitter and receiver were placed face-to-face with a separation distance of 7 mm. To provide the AC excitation signal, a home-made analogical emitter was used, similar to the one used for the therapy-imaging platform described in reference [14]. Charge preamplifier circuit from Cooknell electronics ltd. (CA7/c model with 250 mV/pC gain) was used to drive the electrical signal delivered by the receiver. Signals were acquired with Picoscope 2000 series acquisition card (12 bits resolution and 20 MHz sampling frequency) placed on the receiving end. The time domain and frequency domain response of the transmitted signals are plotted in Figure 7 and Figure 8, no average was applied to the signals. Principally, CMUT is emphasized as a microphone based on its design, which works far away from its resonance frequency band. For the five excitation frequencies, the received signal has significant voltage amplitude, with a spectrum clearly shifted to higher frequencies as the excitation frequency increases.

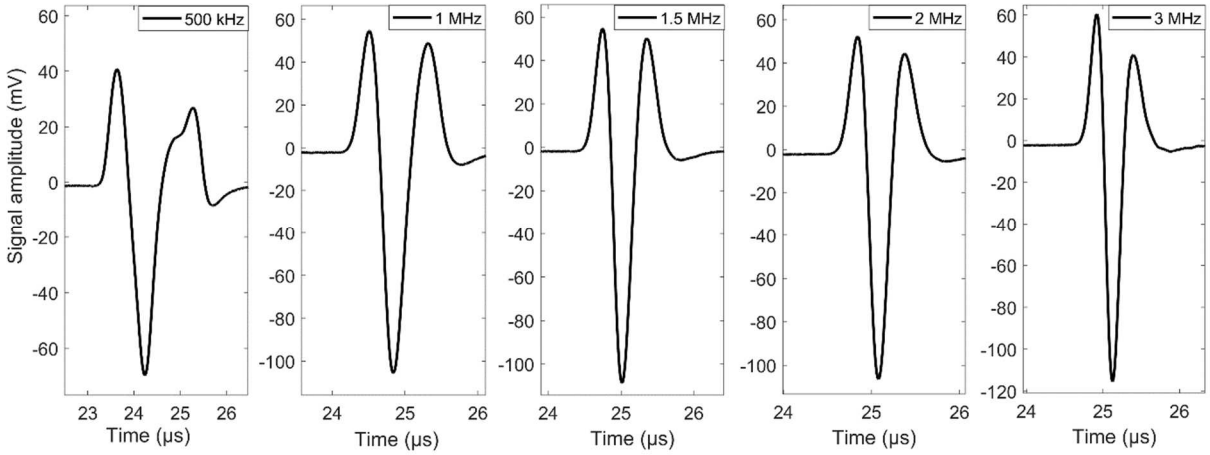

Figure 7 : Time domain response of the transmitted signal for different excitation frequencies

Moreover, the -6 dB relative FBW of the received signals clearly follows the ones of the excitation signal. For example, at 1 MHz, 105 % FBW was measured. At 500 kHz and 1 MHz, a spectral contribution arising from non-linear intrinsic behaviour of CMUT has been observed, similarly at 1.5 MHz respectively. For 2 MHz and 3 MHz excitation frequencies, there is a gain in high frequency components, but attenuation in air compensated for this frequency shifting meaning that the frequency where the maximum occurs remain at 1.5 MHz.

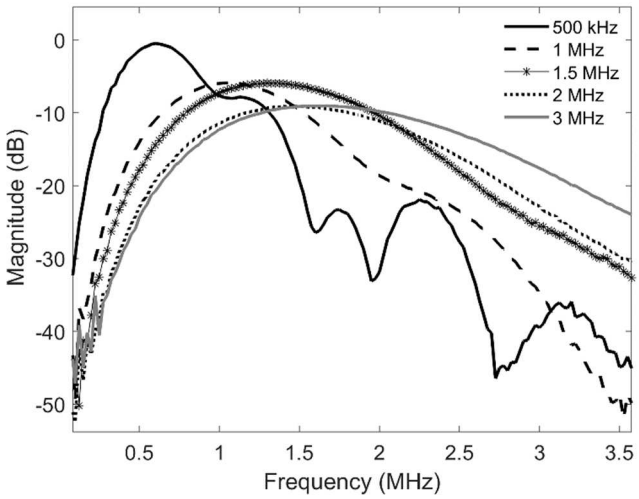

Figure 8 : Frequency domain response of the transmitted signal for different excitation frequencies

The second step of this characterisation was to assess the maximum working distance between emitter and receiver, not for the application targeted in this study, but for potential future applications. The experiments were done at 1 MHz excitation frequency. The emitter was kept

at fixed position while the receiver has moved along the emitter axis from 5 mm to 250 mm. Data acquisition conditions were kept similar as of the previous experiments. The set of impulse responses received are gathered and plotted in Figure 9. The corresponding frequency domain responses for 5 mm, 100 mm and 220 mm are plotted in Figure 10. With the obtained data, it is clear that the Limit Of Detection (LOD) in terms of distance for this device is 220 mm maximum, beyond that the signal-to-noise ratio was not high enough. The received signal shows 30 dB of dynamic with the pulse shape that is clearly centered at 1 MHz and shifts toward lower frequencies when the distance increases, due to acoustic attenuation in air. Although these CMUTs were not designed to attain the optimized sensitivity at larger distances but with the frequency bandwidth, the maximum working distance experiment performed using pulse-echo mode paves the way for other applications. Furthermore, with the obtained data, it is clear that this setup can be used for imaging applications in air, based on its exceptional performances in terms of lateral and axial resolution. In addition, works are currently under investigation to perform imaging tests based on the Synthetic Aperture Focusing Technic beamforming strategy [17], [61], [62].

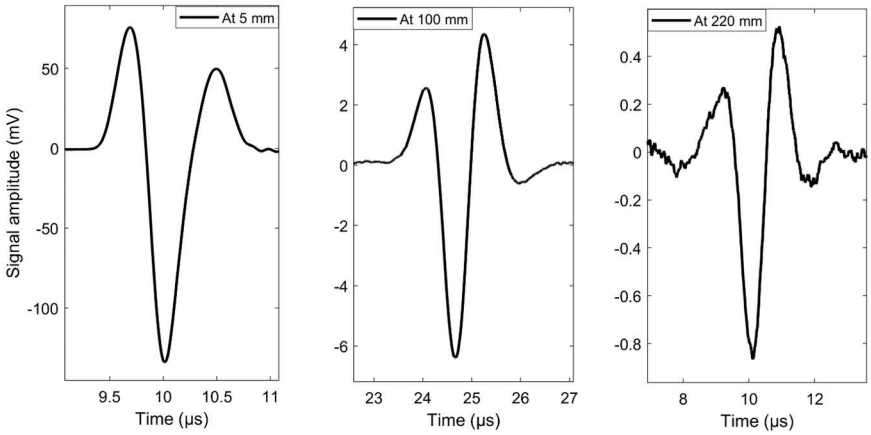

Figure 9: Time-domain signals received for a travelling distance ranging from 5 mm to 220 mm at the excitation frequency of 1 MHz

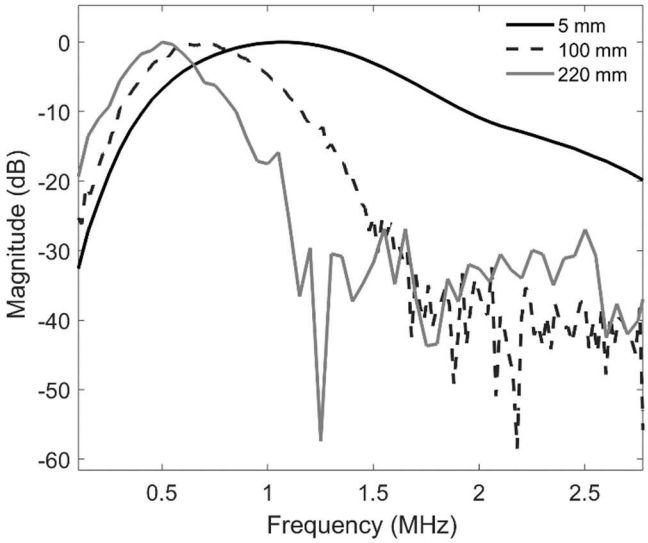

Figure 10: Frequency response of the received signal for 5 mm, 10 mm and 220 mm working distances between emitter and receiver, excitation frequency of 1 MHz

IV. TIME-OF-FLIGHT IN GAS MEDIUM

A. Time-of-flight setup

The fabricated gas sensor unit was tested using a specific test-bench dedicated to the characterization of binary gas mixtures as shown in Figure 11. For the experiments presented in this paper, two binary mixtures were tested: carbon dioxide (CO_2) or hydrogen (H_2) in nitrogen (N_2). Nitrogen was chosen as the reference gas because it has an acoustic velocity close to that of air at room temperature. The test-bench therefore includes three gas tanks (CO_2, H_2 and N_2) and electro-valves controlled by a Labview programme allowing binary mixtures (CO_2/N_2 or H_2/N_2) to be made with chosen concentrations.

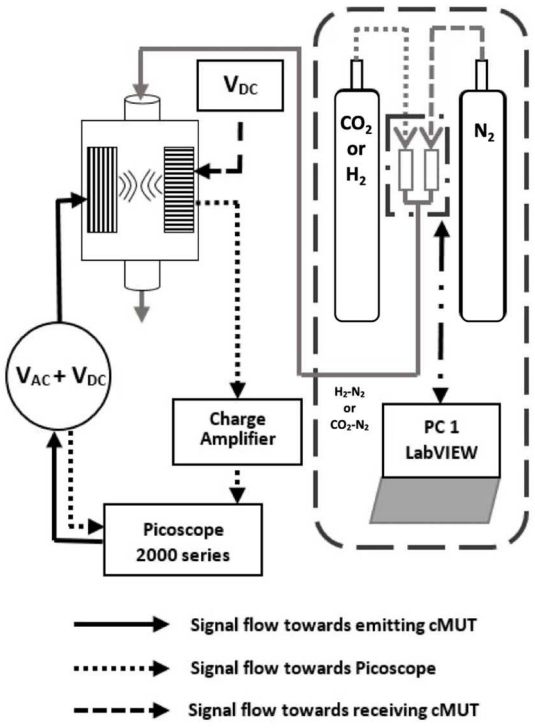

Figure 11: Diagram of the test-bench used for the characterization of binary gas mixtures

As explained in the introduction, the sensor is based on the measurement of time of flight (ToF) variations that depend on the speed of sound in the gas mixture. To give an order of magnitude of the time variations to be measured, the values of the ToF for an acoustic wave to travel a distance of 7 mm in the three pure gases (CO_2, H_2 and N_2) are given in Table 3. It should be noted that the ToF difference between pure CO_2 and pure N_2 is only 6 µs, which means that it is necessary to be able to measure very small ToF variations to accurately monitor the concentration of the binary mixture.

Table 3: Physical properties of CO_2, N_2 and H_2 gases [63]–[65]

Gas	Density ρ (kg/m^3)	Isobar Specific Heat c_p (J/°C.mol)	Isochoric Specific Heat c_v (J/°C.mol)	Velocity C (m/s)	Expected time of flight for pure gas (µs) at d ≈ 7 mm
CO_2	1.82	37.1	28.8	267	26
N_2	1.16	29.1	20.8	349	20
H_2	0.083	28.9	20.5	1306	5.4

To check the initial working conditions, a first measurement was done by filling the cell with pure N_2 and then with pure CO_2. To carry out this experiment, the overall voltage was kept at

90% of V_c with the bias V_{DC}=32 V and the alternative component V_{AC}=20.5 V (41 V peak-to-peak). The frequency is 1.5 MHz, as it corresponds to maximum of the spectrum amplitude (see Figure 8). The bandwidth has been deliberately reduced to avoid energy transmission in the frequency band that is not used in the reception mode (attenuation losses). The emitted signal has therefore been modified: it is a sine burst of 1.5 period instead of 1 period.

The data acquisition duration has been chosen longer than previously to be able to see the forward contribution from emitter to receiver (Figure 12). Note that the receiver signals for both N_2 and CO_2 are clearly separated from the emission, meaning that the duration of the transducer impulse response is small enough to accurately monitor the ToF variations.

The reception occurs after a delay τ which depends on the gas since a difference between pure N_2 and pure CO_2 is clearly observed, with a value close to the expected one of 6 µs. For intermediate CO_2 concentration values, it was chosen to detect the transit time between emission and reception. A standard method based on the detection of the position of the minimum of the signal was used to identify the ToF shift. Since the sampling frequency was high enough (20 MHz), it was possible to interpolate data [39] between two sampling points, resulting in a noise standard deviation of 6 ns instead of 20 ns without interpolation. As expected, the shape of the received signal is slightly different from the results shown in Figure 7 since the excitation signal was longer.

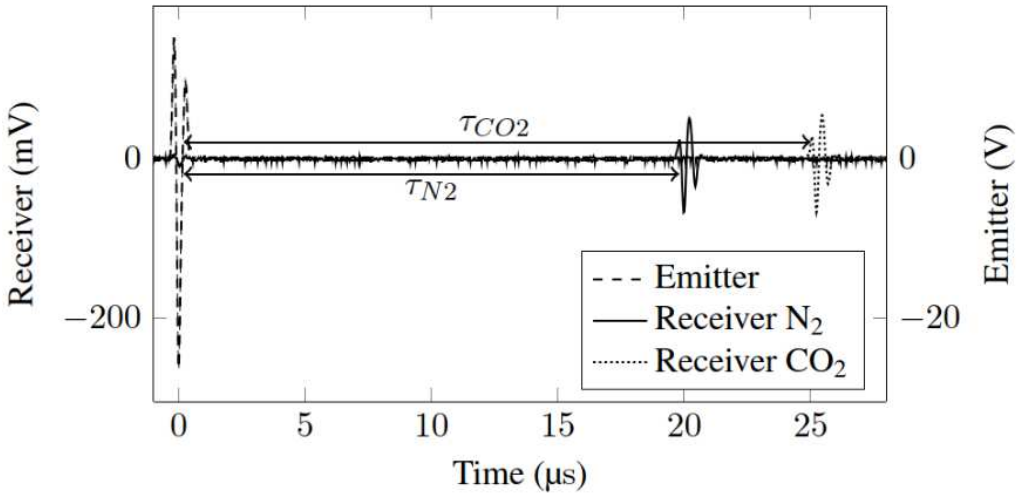

Figure 12 : Alternative part of the reception signal (V_{DC} = 32 V, V_{AC} = 20.5 V) under pure N_2 (solid line) and pure CO_2 (dotted line)

B. Time-of-flight in binary gas mixture

As a first proof of concept, tests were carried out for the binary mixture (CO_2/N_2) with concentration steps from 20 % to 100 %. Between each step, pure N_2 is sent to the measuring cell to show the reversibility of the sensor. Using a set of mass-flow controllers (Brooks 5850S), the gas flow is kept constant at 100±0.7 $cm^3.min^{-1}$ with a stabilization time of about 45s. The temperature T is kept at 20±2 °C. The results (Figure 13.a) clearly show that the proposed setup using two CMUTs to measure ToF allows a change in the gas composition to be detected. The average relative ToF values as a function of the concentration steps are shown in Figure 13.b. In order to confirm the correlation between the sensor output and the gas concentration, the relative changes in ToF have been determined theoretically (Figure 13.b).

Although a detailed demonstration (refer Appendix) is out of this scope, it can be shown that the relative change in the ToF of a gas with respect to N_2 is given by:

$$\frac{d\tau}{\tau} = 1 - \frac{C}{C_{N2}}, \qquad \text{Eq. 4}$$

where C_{N2} and C are the sound velocity under pure N_2 and binary mixture, respectively. C depends on the molar fraction of the targeted gas (CO_2 or H_2) x_G according to:

$$C = \sqrt{\frac{x_G c_{p,G} + (1-x_G) c_{p,N2}}{x_G c_{v,G} + (1-x_G) c_{v,N2}} \frac{P_0}{x_G \rho_G + (1-x_G) \rho_{N2}}} \qquad \text{Eq. 5}$$

where ρ, c_p and c_v are mass density, the isobar heat capacity and the isochoric heat capacity, respectively. For all properties, the subscripts G and N_2 designate the targeted gas (CO_2 or H_2) and N_2, respectively. All these parameters are given in Table 3.

In the same way (full demonstration in the Appendix), for x_G close to zero the sensitivity S_0 is given by:

$$S_0 = \frac{1}{x_G} \cdot \frac{d\tau}{\tau} = \frac{1}{2}\left(\frac{\rho_G}{\rho_{N2}} + \frac{c_{v,G}}{c_{v,N2}} - \frac{c_{p,G}}{c_{p,N2}} - 1 \right) \qquad \text{Eq. 6}$$

The good agreement between theory and experiment confirms that the variations of the output are mainly due to changes in gas concentration. A slight deviation can be noted which results in a smaller sensitivity than the theoretical one. There are two possible reasons for this small

discrepancy. The first is due to the method used to monitor the ToF variations, i.e. the method based on detecting the minimum peak position of the received pulse. Although this aspect is out of the scope of this paper, a potential solution would be to make the detection system more robust by implementing, for example, a cross-correlation detection. The second possible reason for the discrepancy between theory and experiment is the initial ToF value, 20 µs was chosen. In practice; it is difficult to obtain an exact value of the initial ToF because the distance between the emitter and the receiver as well as the initial ultrasonic velocity must be known acurately. So, obtaining an absolute value of the initial time-of-flight requires an extremely complex protocol, using a second reference signal. The implementation of such method is clearly out of scope for this investigation. Practically, implementing a calibration procedure, from which the sensitivity parameter is determined, is preferable.

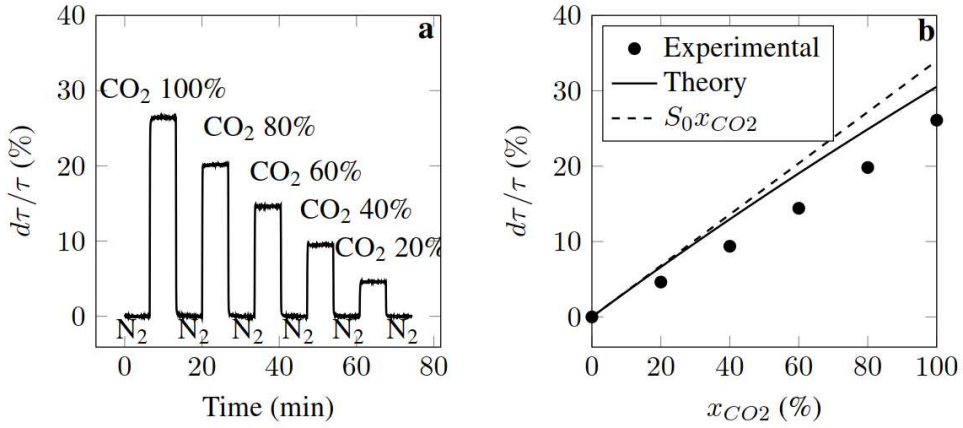

Figure 13 : Measured relative change in τ for different values of x_{CO2} (100%, 80%, 60%, 40% and 20%). (a) As a function of time (V_{DC} = 32V, V_{AC} = 20.5V). (b) As a function of x_{CO2} (dots) with theoretical values of Eq. 5 (solid line) and the tangent at the origin from Eq. 6 (dashed line)

In order to characterise the proposed method for lower concentration, mixtures of either H_2 or CO_2 in N_2 were tested at different low concentration values (4%, 1%, 2%, 3% and 4%). The results are shown in Figure 14. A drift that is too small to be noticed for high concentrations can now be appreciated and is consistent with temperature variations dT below 1°C according to Eq. 7 (refer Appendix for demonstration). After removing such drift by a simple polynomial fitting, the calibration curves were obtained and are shown in Figure 15.

$$\frac{d\tau}{\tau} = -\frac{1}{2}\frac{dT}{T} \qquad \text{Eq. 7}$$

These results highlight a key feature for the sensor: its output varies linearly with the physical quantity to be detected, as long as the relative variations are only a few percent. Despite the

simplicity of the model (ideal gas, small concentrations) and detection method, the sensitivity values (magnitude and sign) remain consistent with the ones obtained by using the Eq. 5 ($3.4x10^{-3}$/% for CO_2 and $-7.1x10^{-3}$/% for H_2).

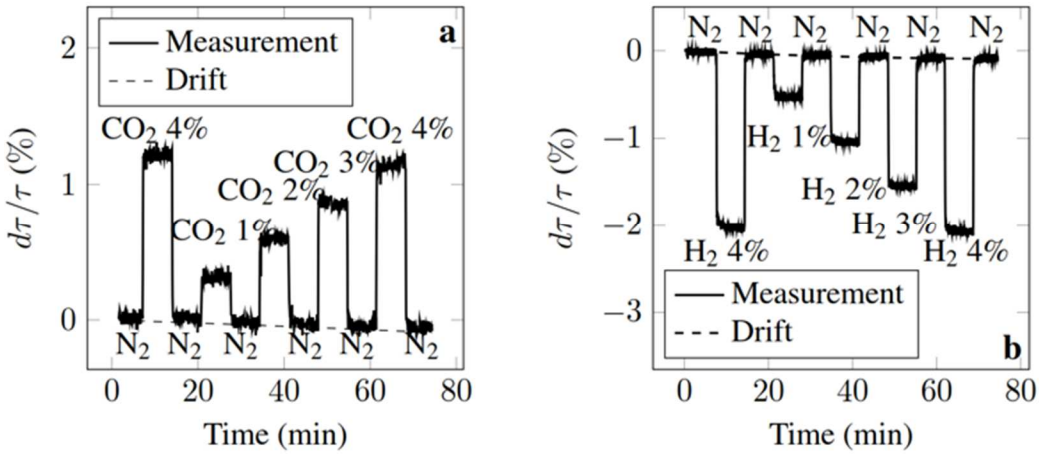

Figure 14: Measured relative change in τ by alternating pure N_2 and either CO_2 (a) or H_2 (b) at different concentrations (4% 1% 2% 3% and 4%)

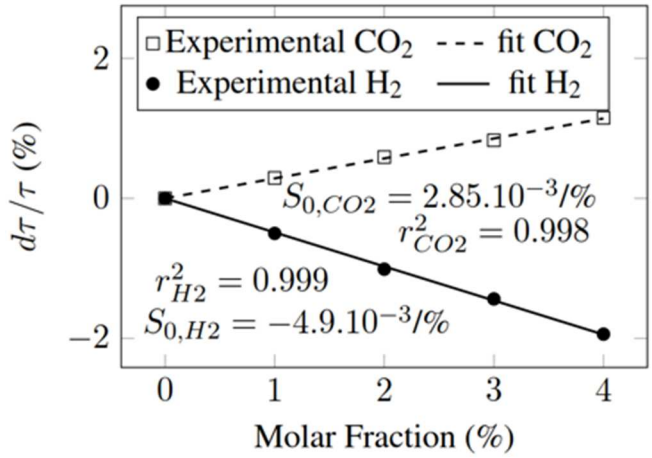

Figure 15: Sensor output characteristics for CO_2 (dashed line) and H_2 (solid line)

From the results of Figure 15, it is possible to estimate the LOD using [66]:

$$\mathrm{LOD} = \frac{3\sigma}{S_0} \qquad \text{Eq. 8}$$

Where $\sigma = 29x10^{-5}$ is the noise standard deviation of the measurement of $d\tau/\tau$. Since the LOD depends on S_0, its value depends on the targeted gas. The estimated values for H_2 and CO_2 are approximately 0.15% and 0.3%, respectively. In order to verify them experimentally, similar experiments as the ones of Figure 14 were performed with the appropriate concentrations and the results are presented in Figure 16.

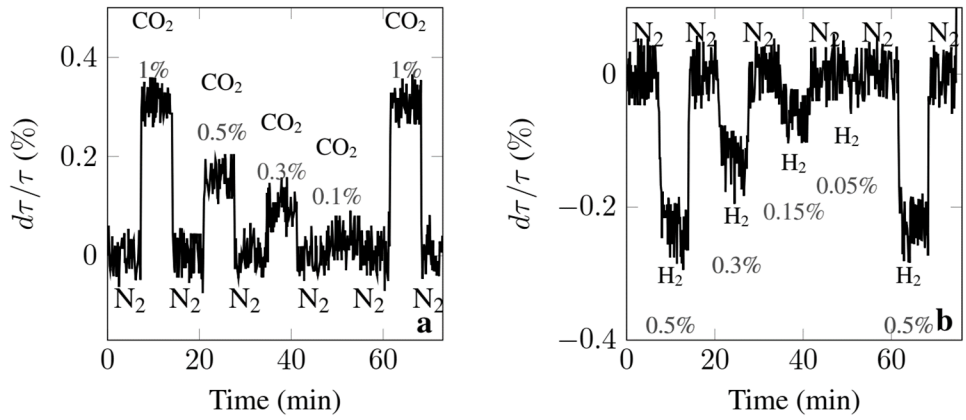

Figure 16: Measured relative change in τ (drift removed) by alternating pure N_2 and either CO_2 (a) at 1 %, 0.5 %, 0.3 %, 0.1 % and 1 % or H_2 (b) at 0.5 %, 0.3 %, 0.15 %, 0.05 % and 0.5 %. These concentrations were chosen to estimate the LOD for CO_2 and H_2

These measurements validate the calculated values for the LOD. A summary of the experimental sensor performance parameters is presented in Table 4.

Table 4: Summary of the experimental sensor performance

Gas	S_0 (10^{-3}/%)	LOD (%)
CO_2	2.85	0.3
H_2	-4.9	0.15

V. CONCLUSION AND PERSPECTIVE

A new approach for binary gas mixture monitoring using uncoated sensors was investigated and demonstrated. The developed method is based on the gas acoustic properties measurement, i.e. the ultrasound velocity, combining usual ToF detection principle and ultra-wide bandwidth air-coupled capacitive micromachined ultrasonic transducers. Air-coupled CMUT were designed as microphone in order to reach FBW higher than 50 %. Experimental results, based on fabricated prototypes, demonstrated the approach relevancy since FBW higher than 100 % were obtained, with a tunable central frequency, from 500 kHz up to 2 MHz. The performance in terms of signal-to-noise ratio showed that, with the fabricated prototype, a working distance of a few centimeters is possible. This paves the way for new applications such as acoustic imaging in air.

The ToF measurements performed with these first prototypes have proven that this technique is suitable to monitor accurately binary gas mixtures. In this paper, CO_2 in N_2 and H_2 in N_2 were tested but it can be widely used for other gas mixtures. Sensor performance was evaluating by measuring both the sensitivity at low gas concentration values and the limit of detection (LOD). For both gas mixtures, the experimental sensitivity is generally in agreement with the theoretical value despite deviations that could possibly be reduced by improving the detection algorithm. In the case of H2 detection, concentration lower than 0.15 % have been detected.

It is certain that this LOD value is not competitive with that of the state of the art of coated sensors. However, the approach presented in this paper shows a good trade-off to meet simultaneously good accuracy, simplified fabrication method, high integrability level and high reliability. This homemade setup is portable. The sensor performance can be improved in two ways: i) using optimized electronic driving circuits in reception, ii) using a wafer bonding process, since it enhances the homogeneity of CMUTs and the active surface ratio too.

VI. ANNEX : theoretical determination of the relative time-of-flight variations

The Time of Flight τ depends on both the sound velocity of the gas *C* and the distance *d* between the emitter and the receiver:

$$\tau = \frac{d}{C} \qquad \text{Eq. A.1}$$

The relationship between the gas properties and the sound velocity *C* is given by Newton-Laplace formula [67]:

$$C = \sqrt{\frac{\gamma P_0}{\rho}} \qquad \text{Eq. A.2}$$

where P_0 is the static pressure, ρ the mixture mass density and γ the heat capacity ratio. In the case of binary gas mixture, both properties, ρ and γ, depend on the molar fraction of the gas to detect x_G. The mixture gas density in N_2 is given by:

$$\rho = x_G \rho_G + (1 - x_G)\rho_{N2} \qquad \text{Eq. A.3}$$

where ρ_G and ρ_{N2} are the mass density of the pure gas to detect and pure N_2, respectively.

Additionally, the heat capacity ratio is given by Eq. A.4 [68]:

$$\gamma = \frac{x_G c_{p,G} + (1 - x_G) c_{p,N2}}{x_G c_{v,G} + (1 - x_G) c_{v,N2}} \qquad \text{Eq. A.4}$$

Where, $c_{p,G}$, $c_{p,N2}$ are the isobar heat capacity of the pure gas to detect and pure N_2, respectively, $c_{v,G}$ and $c_{v,N2}$ are the isochoric heat capacity of the pure gas to detect and pure N_2, respectively.

By combining Equations A.1 to A.4 it is possible to obtain a equation of the relative change in time of flight, $d\tau/\tau$, when the initial state is pure N_2 (Eq. A.5):

$$\frac{d\tau}{\tau} = \frac{1}{2}\left(\frac{\rho_G - \rho_{N2}}{x_G \rho_G + (1 - x_G)\rho_{N2}} + \frac{c_{v,G} - c_{v,N2}}{x_G c_{v,G} + (1 - x_G) c_{v,N2}} - \frac{c_{p,G} - c_{p,N2}}{x_G c_{p,G} + (1 - x_G) c_{p,N2}} \right) x_G \qquad \text{Eq. A.5}$$

which can be further simplified, in the case x_G << 1 into:

$$\frac{d\tau}{\tau} = \frac{1}{2}\left(\frac{\rho_G}{\rho_{N2}} + \frac{c_{v,G}}{c_{v,N2}} - \frac{c_{p,G}}{c_{p,N2}} - 1 \right) x_G \qquad \text{Eq. A.6}$$

From Eq. A.6, one can define the sensitivity for small concentrations S_0 (x_G as input and $d\tau/\tau$ as output):

$$S_0 = \frac{d\tau}{\tau x_G} = \frac{1}{2}\left(\frac{\rho_G}{\rho_{N2}} + \frac{c_{v,G}}{c_{v,N2}} - \frac{c_{p,G}}{c_{p,N2}} - 1 \right) \qquad \text{Eq. A.7}$$

Defined in such a way, S_0 depends only on the thermodynamic properties of the gases involved and it is independent on the setup.

For an ideal gas, the mass density depends on the static pressure and temperature:

$$\rho = \frac{P_0 M}{RT} \qquad \text{Eq. A.8}$$

Then, assuming that γ is independent of the temperature, the dependence of the ToF to the temperature can be expressed:

$$\frac{d\tau}{\tau} = -\frac{dC}{C} = -\frac{1}{2}\left(\frac{d\gamma}{\gamma} + \frac{dP_0}{P_0} - \frac{d\rho}{\rho} \right) = -\frac{1}{2}\left(\frac{d\gamma}{\gamma} + \frac{dT}{T} \right) \approx -\frac{1}{2}\frac{dT}{T} \qquad \text{Eq. A.9}$$

AUTHOR CONTRIBUTIONS

PS and LI has equally contributed in the paper writing. PS, JFM, DA, LC and DC have designed and fabricated the CMUT and the measuring cell. Further PS and DC has optimized the parameters and made characterisation in air. LI and ID has validated the system by performing ToF modelling and measurement with various binary gas mixtures. All the authors have read and approved the manuscript.

FUNDING

This work has been carried out within the framework of the project H2MEMS, financially supported by the French government's program "Investissements d'Avenir", operated by ANDRA, the French national agency for radioactive waste management.

ACKNOWLEDGEMENTS

The authors thank Flavien BARCELLA from GREMAN laboratory for his technical assistance during creation of the emitter/receiver prototypes.

REFERENCES

[1] Haller and Khuri-Yakub, "A surface micromachined electrostatic ultrasonic air transducer," in *Proceedings of IEEE Ultrasonics Symposium ULTSYM-94*, Cannes, France, 1994, pp. 1241–1244 vol.2, doi: 10.1109/ULTSYM.1994.401810.

[2] M. I. Haller and B. T. Khuri-Yakub, "A surface micromachined electrostatic ultrasonic air transducer," *IEEE Trans. Ultrason., Ferroelect., Freq. Contr.*, vol. 43, no. 1, pp. 1–6, Jan. 1996, doi: 10.1109/58.484456.

[3] O. Oralkan *et al.*, "Capacitive micromachined ultrasonic transducers: next-generation arrays for acoustic imaging?," *IEEE Trans. Ultrason., Ferroelect., Freq. Contr.*, vol. 49, no. 11, pp. 1596–1610, Nov. 2002, doi: 10.1109/TUFFC.2002.1049742.

[4] W. A. N'Djin *et al.*, "Capacitive Micromachined Ultrasound Transducers for Interstitial High-Intensity Ultrasound Therapies," *IEEE Trans. Ultrason., Ferroelect., Freq. Contr.*, vol. 64, no. 8, pp. 1245–1260, Aug. 2017, doi: 10.1109/TUFFC.2017.2707663.

[5] O. Oralkan *et al.*, "Initial pulse-echo imaging results with one-dimensional capacitive micromachined ultrasonic transducer arrays," in *2000 IEEE Ultrasonics Symposium. Proceedings. An International Symposium (Cat. No.00CH37121)*, San Juan, Puerto Rico, 2000, vol. 1, pp. 959–962, doi: 10.1109/ULTSYM.2000.922700.

[6] O. Oralkan *et al.*, "Volumetric ultrasound imaging using 2-D CMUT arrays," *IEEE Trans. Ultrason., Ferroelect., Freq. Contr.*, vol. 50, no. 11, pp. 1581–1594, Nov. 2003, doi: 10.1109/TUFFC.2003.1251142.

[7] B. Belgacem *et al.*, "Optimization of the fabrication of sealed capacitive transducers using surface micromachining," *J. Micromech. Microeng.*, vol. 14, no. 2, pp. 299–304, Feb. 2004, doi: 10.1088/0960-1317/14/2/019.

[8] B. T. Khuri-Yakub and Ö. Oralkan, "Capacitive micromachined ultrasonic transducers for medical imaging and therapy," *J. Micromech. Microeng.*, vol. 21, no. 5, p. 054004, May 2011, doi: 10.1088/0960-1317/21/5/054004.

[9] E. Jeanne *et al.*, "Protection Layer Influence on Capacitive Micromachined Ultrasonic Transducers Performance," *MRS Proc.*, vol. 1052, pp. 1052-DD06-27, 2007, doi: 10.1557/PROC-1052-DD06-27.

[10] J. Lascaud *et al.*, "Investigation of ultrasonic absorption in the MHz frequency range by silicon substrates with a built-in porous silicon layer," *Ultrasonics*, vol. 96, pp. 196–202, Jul. 2019, doi: 10.1016/j.ultras.2019.01.006.

[11] M. Pekař *et al.*, “Frequency Tuning of Collapse-Mode Capacitive Micromachined Ultrasonic Transducer,” *Ultrasonics*, vol. 74, pp. 144–152, Feb. 2017, doi: 10.1016/j.ultras.2016.10.002.

[12] M. Pekař *et al.*, “Quantitative imaging performance of frequency-tunable capacitive micromachined ultrasonic transducer array designed for intracardiac application: Phantom study,” *Ultrasonics*, vol. 84, pp. 421–429, Mar. 2018, doi: 10.1016/j.ultras.2017.11.021.

[13] A. Boulmé *et al.*, “A capacitive micromachined ultrasonic transducer probe for assessment of cortical bone,” *IEEE Transactions on Ultrasonics, Ferroelectrics, and Frequency Control*, vol. 61, no. 4, pp. 710–723, Apr. 2014, doi: 10.1109/TUFFC.2014.2959.

[14] D. Gross *et al.*, “A cMUT probe for ultrasound-guided focused ultrasound targeted therapy,” *IEEE Trans. Ultrason., Ferroelect., Freq. Contr.*, vol. 62, no. 6, pp. 1145–1160, Jun. 2015, doi: 10.1109/TUFFC.2014.006887.

[15] M. M. Mahmud *et al.*, “Improved CMUT structure and method of operation for dual-frequency acoustic angiography,” in *2017 IEEE International Ultrasonics Symposium (IUS)*, Washington, DC, Sep. 2017, pp. 1–4, doi: 10.1109/ULTSYM.2017.8091920.

[16] M. Castaings and B. Hosten, “The use of electrostatic, ultrasonic, air-coupled transducers to generate and receive Lamb waves in anisotropic, viscoelastic plates,” *Ultrasonics*, vol. 36, no. 1–5, pp. 361–365, Feb. 1998, doi: 10.1016/S0041-624X(97)00144-3.

[17] K. K. Park and B. T. Khuri-Yakub, “3-D airborne ultrasound synthetic aperture imaging based on capacitive micromachined ultrasonic transducers,” *Ultrasonics*, vol. 53, no. 7, pp. 1355–1362, Sep. 2013, doi: 10.1016/j.ultras.2013.04.003.

[18] B. Ma *et al.*, “Wide Bandwidth and Low Driving Voltage Vented CMUTs for Airborne Applications,” *IEEE Trans. Ultrason., Ferroelect., Freq. Contr.*, vol. 66, no. 11, pp. 1777–1785, Nov. 2019, doi: 10.1109/TUFFC.2019.2928170.

[19] S. Na *et al.*, “Lumped element modeling of air-coupled capacitive micromachined ultrasonic transducers with annular cell geometry,” *Ultrasonics*, vol. 76, pp. 19–27, Apr. 2017, doi: 10.1016/j.ultras.2016.11.014.

[20] S. Na *et al.*, “Capacitive micromachined ultrasonic transducers based on annular cell geometry for air-coupled applications,” *Ultrasonics*, vol. 71, pp. 152–160, Sep. 2016, doi: 10.1016/j.ultras.2016.06.008.

[21] S. Na *et al.*, “An Optimization and Comparative Study of Air-Coupled CMUT Cells With Circular and Annular Geometries,” *IEEE Trans. Ultrason., Ferroelect., Freq. Contr.*, vol. 64, no. 11, pp. 1723–1734, Nov. 2017, doi: 10.1109/TUFFC.2017.2739692.

[22] W. M. D. Wright and S. G. McSweeney, “A tethered front-plate electrode CMUT for broadband air-coupled ultrasound,” in *2013 IEEE International Ultrasonics Symposium (IUS)*, Prague, Czech Republic, Jul. 2013, pp. 1716–1719, doi: 10.1109/ULTSYM.2013.0437.

[23] H. Toda, “The Precise Mechanisms of a High-Speed Ultrasound Gas Sensor and Detecting Human-Specific Lung Gas Exchange,” *International Journal of Advanced Robotic Systems*, vol. 9, no. 6, p. 249, Dec. 2012, doi: 10.5772/53566.

[24] G. Bui *et al.*, “Two Capacitive Micro-Machined Ultrasonic Transducers for Wind Speed Measurement,” *Sensors*, vol. 16, no. 6, p. 814, Jun. 2016, doi: 10.3390/s16060814.

[25] P. S. Chauhan and S. Bhattacharya, “Hydrogen gas sensing methods, materials, and approach to achieve parts per billion level detection: A review,” *International Journal of Hydrogen Energy*, vol. 44, no. 47, pp. 26076–26099, Oct. 2019, doi: 10.1016/j.ijhydene.2019.08.052.

[26] K. K. Park *et al.*, “Capacitive micromachined ultrasonic transducers for chemical detection in nitrogen,” *Appl. Phys. Lett.*, vol. 91, no. 9, p. 094102, Aug. 2007, doi: 10.1063/1.2776348.

[27] K. K. Park *et al.*, “Capacitive micromachined ultrasonic transducer (CMUT) as a chemical sensor for DMMP detection,” *Sensors and Actuators B: Chemical*, vol. 160, no. 1, pp. 1120–1127, Dec. 2011, doi: 10.1016/j.snb.2011.09.036.

[28] S. Eaimkhong, “Label-Free Biodetection Using Capacitive Micromachined Ultrasonic Transducers (CMUTs) and Its Application for Cardiovascular Disease Diagnostics,” *Journal of Nanomedicine & Nanotechnology*, vol. 03, no. 05, 2012, doi: 10.4172/2157-7439.1000144.

[29] M. M. Mahmud *et al.*, “A low-power gas sensor for environmental monitoring using a capacitive micromachined ultrasonic transducer,” Nov. 2014, pp. 677–680, doi: 10.1109/ICSENS.2014.6985089.

[30] D. Barauskas *et al.*, “CMUT for high sensitivity greenhouse gas sensing,” Oct. 2015, pp. 1–4, doi: 10.1109/ULTSYM.2015.0472.

[31] C. Seok *et al.*, “A battery-operated wireless multichannel gas sensor system based on a capacitive micromachined ultrasonic transducer (CMUT) array,” Oct. 2016, pp. 1–3, doi: 10.1109/ICSENS.2016.7808803.

[32] M. M. Mahmud *et al.*, "Gravimetric biosensor based on a capacitive micromachined ultrasonic transducer functionalized with peptide ligands," in *2017 IEEE SENSORS*, Glasgow, Oct. 2017, pp. 1–3, doi: 10.1109/ICSENS.2017.8234352.

[33] S. Park *et al.*, "CMUT-based resonant gas sensor array for VOC detection with low operating voltage," *Sensors and Actuators B: Chemical*, vol. 273, pp. 1556–1563, Nov. 2018, doi: 10.1016/j.snb.2018.07.043.

[34] I. Dufour *et al.*, "Unconventional uses of microcantilevers as chemical sensors in gas and liquid media," *Sensors and Actuators B: Chemical*, vol. 170, pp. 115–121, Jul. 2012, doi: 10.1016/j.snb.2011.02.050.

[35] M. T. Boudjiet *et al.*, "New characterization methods for monitoring small resonant frequency variation: Experimental tests in the case of hydrogen detection with uncoated silicon microcantilever-based sensors," *Sensors and Actuators B: Chemical*, vol. 199, pp. 269–276, Aug. 2014, doi: 10.1016/j.snb.2014.03.098.

[36] L. Iglesias *et al.*, "Proof of Concept and Preliminary Results of Gas Detection by Measuring the Admittance at the Resonance and Anti-resonance of an Uncoated CMUT," *Front. Mech. Eng.*, vol. 6, p. 14, Mar. 2020, doi: 10.3389/fmech.2020.00014.

[37] I. Dufour *et al.*, "Resonant MEMS for Gas Detection Based on the Measurements of Physical Properties of Gas Mixtures," in *2020 Joint Conference of the IEEE International Frequency Control Symposium and International Symposium on Applications of Ferroelectrics (IFCS-ISAF)*, Keystone, CO, USA, Jul. 2020, pp. 1–3, doi: 10.1109/IFCS-ISAF41089.2020.9234908.

[38] J. Coulthard, "Ultrasonic cross-correlation flowmeters," *Ultrasonics*, vol. 11, no. 2, pp. 83–88, Mar. 1973, doi: 10.1016/0041-624X(73)90406-X.

[39] Xiaoming Lai and H. Torp, "Interpolation methods for time-delay estimation using cross-correlation method for blood velocity measurement," *IEEE Trans. Ultrason., Ferroelect., Freq. Contr.*, vol. 46, no. 2, pp. 277–290, Mar. 1999, doi: 10.1109/58.753016.

[40] P. G. M. de Jong *et al.*, "Determination of Tissue Motion Velocity by Correlation Interpolation of Pulsed Ultrasonic Echo Signals," *Ultrason Imaging*, vol. 12, no. 2, pp. 84–98, Apr. 1990, doi: 10.1177/016173469001200202.

[41] D. E. Chimenti, "Review of air-coupled ultrasonic materials characterization," *Ultrasonics*, vol. 54, no. 7, pp. 1804–1816, Sep. 2014, doi: 10.1016/j.ultras.2014.02.006.

[42] L. Pizarro *et al.*, “Airborne ultrasonic electrostatic transducers with conductive grooved backplates: tailoring their centre frequency, sensitivity and bandwidth,” *Ultrasonics*, vol. 37, no. 7, pp. 493–503, Nov. 1999, doi: 10.1016/S0041-624X(99)00033-5.

[43] Sylvain Hallereau and Nicolas Radufe, “TDK-Chirp CH101 Ultrasonic Time of Flight Sensor,” p. 113, Feb. 2020.

[44] David Horsley, “World’s first MEMS ultrasonic time-of-flight sensors,” *Technologies & Products Press Conference 2018*, Nov. 14, 2018.

[45] S. Alasatri *et al.*, “AlN-on-Si Square Diaphragm Piezoelectric Micromachined Ultrasonic Transducer with Extended Range of Detection,” *Proceedings*, vol. 2, no. 13, p. 913, Nov. 2018, doi: 10.3390/proceedings2130913.

[46] G.-H. Feng and H.-J. Liu, “Piezoelectric Micromachined Ultrasonic Transducers with a Cost-Effective Bottom-Up Fabrication Scheme for Millimeter-Scale Range Finding,” *Sensors*, vol. 19, no. 21, p. 4696, Oct. 2019, doi: 10.3390/s19214696.

[47] L. Kang *et al.*, “Flow Velocity Measurement Using a Spatial Averaging Method with Two-Dimensional Flexural Ultrasonic Array Technology,” *Sensors*, vol. 19, no. 21, p. 4786, Nov. 2019, doi: 10.3390/s19214786.

[48] S. Kumar and H. Furuhashi, “Long-range measurement system using ultrasonic range sensor with high-power transmitter array in air,” *Ultrasonics*, vol. 74, pp. 186–195, Feb. 2017, doi: 10.1016/j.ultras.2016.10.012.

[49] S. T. Hansen *et al.*, “Improved modeling and design of microphones using radio frequency detection with capacitive micromachined ultrasonic transducers,” in *2001 IEEE Ultrasonics Symposium. Proceedings. An International Symposium (Cat. No.01CH37263)*, Atlanta, GA, USA, 2001, vol. 2, pp. 961–964, doi: 10.1109/ULTSYM.2001.991879.

[50] M. Pedersen *et al.*, “An integrated silicon capacitive microphone with frequency-modulated digital output,” *Sensors and Actuators A: Physical*, vol. 69, no. 3, pp. 267–275, Sep. 1998, doi: 10.1016/S0924-4247(98)00092-2.

[51] J. J. Neumann and K. J. Gabriel, “CMOS-MEMS membrane for audio-frequency acoustic actuation,” *Sensors and Actuators A: Physical*, vol. 95, no. 2–3, pp. 175–182, Jan. 2002, doi: 10.1016/S0924-4247(01)00728-2.

[52] Y. Je *et al.*, “The impact of micromachined ultrasonic radiators on the efficiency of transducers in air,” *Ultrasonics*, vol. 53, no. 6, pp. 1124–1134, Aug. 2013, doi: 10.1016/j.ultras.2013.02.008.

[53] T. M. Khan *et al.*, “High-Intensity Airborne CMUT Transmitter Array With Beam Steering,” *J. Microelectromech. Syst.*, vol. 29, no. 6, pp. 1537–1546, Dec. 2020, doi: 10.1109/JMEMS.2020.3026094.

[54] P. Shanmugam *et al.*, “CMUT Based Air Coupled Transducers for Gas-Mixture Analysis,” in *2018 IEEE International Ultrasonics Symposium (IUS)*, Kobe, Japan, Oct. 2018, pp. 1–4, doi: 10.1109/ULTSYM.2018.8579789.

[55] D. Certon *et al.*, “Low frequency cMUT technology: Application to measurement of brain movement and assessment of bone quality,” *IRBM*, vol. 34, no. 2, pp. 159–166, Apr. 2013, doi: 10.1016/j.irbm.2013.01.009.

[56] A. S. Erguri *et al.*, and B. T. Khuri-Yakub, “Capacitive micromachined ultrasonic transducers: fabrication technology,” *IEEE Transactions on Ultrasonics, Ferroelectrics and Frequency Control*, vol. 52, no. 12, pp. 2242–2258, Dec. 2005, doi: 10.1109/TUFFC.2005.1563267.

[57] J. Heller *et al.*, “Performance Evaluation of CMUT-Based Ultrasonic Transformers for Galvanic Isolation,” *IEEE Transactions on Ultrasonics, Ferroelectrics, and Frequency Control*, vol. 65, no. 4, pp. 617–629, Apr. 2018, doi: 10.1109/TUFFC.2018.2796303.

[58] N. Sénégond *et al.*, “High voltage time domain response of cMUT membrane: Laser interferometry measurements,” *Physics Procedia*, vol. 3, no. 1, pp. 1011–1016, Jan. 2010, doi: 10.1016/j.phpro.2010.01.130.

[59] N. Senegond *et al.*, “Fast time-domain modeling of fluid-coupled cMUT cells: from the single cell to the 1-D linear array element,” *IEEE Trans. Ultrason., Ferroelect., Freq. Contr.*, vol. 60, no. 7, pp. 1505–1518, Jul. 2013, doi: 10.1109/TUFFC.2013.2723.

[60] D. Certon *et al.*, “A finite difference model For cMUT devices,” *IEEE Trans. Ultrason., Ferroelect., Freq. Contr.*, vol. 52, no. 12, pp. 2199–2210, Dec. 2005, doi: 10.1109/TUFFC.2005.1563263.

[61] J. T. Ylitalo and H. Ermert, “Ultrasound synthetic aperture imaging: monostatic approach,” *IEEE Trans. Ultrason., Ferroelect., Freq. Contr.*, vol. 41, no. 3, pp. 333–339, May 1994, doi: 10.1109/58.285467.

[62] S. Takahashi and H. Ohigashi, “Ultrasonic imaging using air-coupled P(VDF/TrFE) transducers at 2MHz,” *Ultrasonics*, vol. 49, no. 4–5, pp. 495–498, May 2009, doi: 10.1016/j.ultras.2008.10.020.

[63] *Engineering ToolBox*. https://www.engineeringtoolbox.com/.

[64] *Gas encyclopedia air liquide*. https://encyclopedia.airliquide.com/.

[65] A. J. Zuckerwar, *Handbook of the speed of sound in real gases. Volume III, Volume III,*. Amsterdam; Boston: Academic Press, 2002.

[66] D. Lange *et al.*, "Complementary Metal Oxide Semiconductor Cantilever Arrays on a Single Chip: Mass-Sensitive Detection of Volatile Organic Compounds," *Anal. Chem.*, vol. 74, no. 13, pp. 3084–3095, Jul. 2002, doi: 10.1021/ac011269j.

[67] M. Suchenek and T. Borowski, "Measuring Sound Speed in Gas Mixtures Using a Photoacoustic Generator," *Int J Thermophys*, vol. 39, no. 1, p. 11, Jan. 2018, doi: 10.1007/s10765-017-2335-2.

[68] A. K. Law *et al.*, "Effect of Diffusion on Ultrasonic Attenuation in Mixtures of the Rare Gases," *The Journal of the Acoustical Society of America*, vol. 41, no. 1, pp. 93–99, Jan. 1967, doi: 10.1121/1.1910336.